HHS Public Access

Author manuscript

Cell Rep. Author manuscript; available in PMC 2017 October 03.

Published in final edited form as:

Cell Rep. 2017 July 18; 20(3): 721–736. doi:10.1016/j.celrep.2017.06.074.

Proteomic and metabolomic characterization of a mammalian cellular transition from quiescence to proliferation

Ho-Joon Lee[1,10,11], **Mark P. Jedrychowski**[2,10], **Arunachalam Vinayagam**[4,10], **Ning Wu**[5], **Ng Shyh-Chang**[6], **Yanhui Hu**[4], **Chua Min-Wen**[6], **Jodene K. Moore**[1], **John M. Asara**[7], **Costas A. Lyssiotis**[3], **Norbert Perrimon**[4], **Steven P. Gygi**[2], **Lewis C. Cantley**[8], and **Marc W. Kirschner**[1,*,9]

[1]Department of Systems Biology, Harvard Medical School, Boston, MA 02115, USA

[2]Department of Cell Biology, Harvard Medical School, Boston, MA 02115, USA

[3]Department of Molecular and Integrative Physiology and Department of Internal Medicine, Division of Gastroenterology, University of Michigan Medical School, Ann Arbor, MI 48109, USA

[4]Department of Genetics, Harvard Medical School, Boston, MA 02115, USA

[5]Center for Cancer and Cell Biology, Van Andel Research Institute, Grand Rapids, MI 49503, USA

[6]Stem Cell & Regenerative Biology, Genome Institute of Singapore, S138672, Singapore

[7]Division of Signal Transduction, Department of Medicine, Beth Israel Deaconess Medical Center and Harvard Medical School, Boston, MA, 02115, USA

[8]Meyer Cancer Center, Department of Medicine, Weill Cornell Medical College, New York, NY 10065, USA

SUMMARY

There exist similarities and differences in metabolism and physiology between normal proliferative cells and tumor cells. Once a cell enters the cell cycle, metabolic machinery is engaged to facilitate various processes. The kinetics and regulation of these metabolic changes have not been properly evaluated. To correlate the orchestration of these processes with the cell cycle, we analyzed the transition from quiescence to proliferation of a non-malignant murine pro-B lymphocyte cell line in response to IL-3. Using multiplex mass-spectrometry-based proteomics

[*]**CORRESPONDING AUTHOR**. Marc W. Kirschner, marc@hms.harvard.edu.

[9]**LEAD CONTACT**

Marc W. Kirschner, marc@hms.harvard.edu

[10]These authors contributed equally.

[11]Present address

Department of Molecular and Integrative Physiology, University of Michigan Medical School, Ann Arbor, MI 48109, USA

AUTHOR CONTRIBUTIONS

HJL, MPJ, SPG, LCC, and MWK performed proteomics experiments and data analysis and interpretation. HJL, CAL, JMA, LCC, and MWK performed metabolomics experiments and data analysis and interpretation. HJL, VA, YH, NP, and MWK performed protein module analysis and data interpretation. HJL and JKM performed flow cytometry. HJL, NW, NSC, and CMW performed Western blotting. HJL, MPJ, CAL, VA, and MWK wrote the paper.

we show that the transition to proliferation shares features generally attributed to cancer cells: up-regulation of glycolysis, lipid metabolism, amino-acid synthesis, and nucleotide synthesis and down-regulation of oxidative phosphorylation and the urea cycle. Furthermore, metabolomic profiling of this transition reveals similarities to cancer-related metabolic pathways. In particular, we find that methionine is consumed at a higher rate than other essential amino acids, with a potential link to epigenetic maintenance.

eTOC Blurb

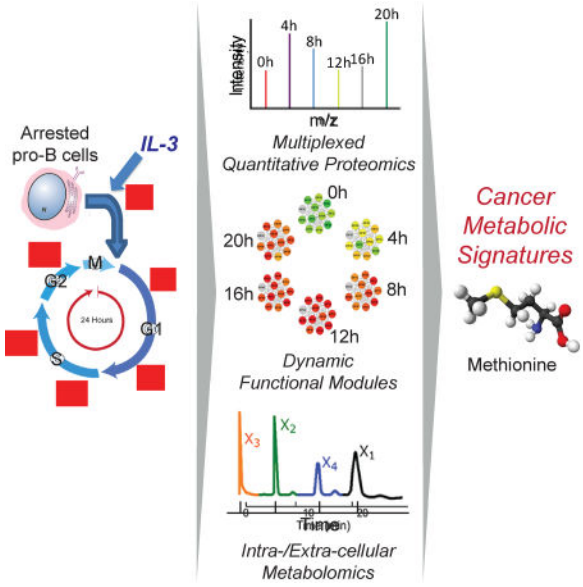

Lee et al. generate and integrate quantitative time-course proteomic and metabolomic profiling data to find that global metabolic reprogramming of an IL-3 activation resembles metabolic rewiring in cancer with high consumption of methionine in G1.

INTRODUCTION

In addition to nutrients mammalian cells require extracellular growth factors to grow and proliferate (Conlon and Raff, 1999; Pardee, 1989; Sherr, 1994; Zetterberg, 1990). Absent such factors, many types of cells survive in a quiescent or G0 state. Re-introduction of growth factors will drive these cells into the cell cycle. This process which leads to a change of cell state has intrigued researchers from the early days of mammalian cell culture. Numerous experiments have been performed with serum deprivation/reintroduction protocols to study the kinetics of how cells in the G0 state re-enter the cell cycle (Planas-Silva and Weinberg, 1997; Zetterberg et al., 1995). In recent proteomic studies T-cell activation was used to characterize specifically nuclear and mitochondrial changes as cells transitioned from G0 to G1 (Orr et al., 2012; Ron-Harel et al., 2016). While these experiments identified several cellular behaviors, we believed that a more global search of protein expression could lead to more complete understanding of this important transition. Today many of the obstacles to proteome-wide quantitative mass spectrometry (MS) have been overcome, but the issues of depth of proteomic coverage still remains with some

classes of abundant proteins easily measured and other rarer proteins like receptors, secreted signaling molecules and transcription factors under-sampled. Yet for many protein families and pathways, the coverage is good enough to be confident about making solid generalizations. This is particularly true for the very abundant metabolic enzymes, which can provide comprehensive insights into the state of cellular metabolism.

We have characterized the cytokine-mediated transition of the pro-B lymphocyte cell line, FL5.12 (McKearn et al., 1985), from a quiescent state to a proliferative state at the proteomic level. FL5.12 cells are exclusively dependent on IL-3 for cell growth and proliferation, and can be synchronized in the G0 state by IL-3 removal and induced to proliferate by adding IL-3. As such, they provide a better-controlled experiment relative to addition and removal of the complex mixture of growth factors found in serum. We used an FL5.12 cell line that expresses Bcl-2 to prevent apoptosis when IL-3 is removed for several days (Nuñez et al., 1990). For analysis we have employed a versatile multiplex method for quantitative MS that employs tandem isobaric mass tags that can simultaneously determine the ratio of a given protein in several samples (Singh et al., 2014; Thompson et al., 2003; Ting et al., 2011). We found that the predominant proteomic changes during transition through the cell cycle were metabolic. We bolstered the proteomic studies with mass spectrometry-based metabolomics analyses. Collectively, these revealed that intermediary metabolism in pro-B cell proliferation bears strong similarity to cancer metabolism, including major changes in translation machinery and nucleotide and methionine pathways.

RESULTS

Features of quiescence and cell cycle entry

Cells in the G0 phase of the cell cycle are defined by a lack of proliferation (marked by low Ki-67 and high Cdkn1b/p27 expression), reduced cell size, and active autophagy. Reduced metabolic activity or flux rates are not always a hallmark of the quiescent state (Lemons et al., 2010). IL-3-deprived FL5.12 cells meet several of the qualifications for the G0 state. After 36 hours of IL-3 depletion, FL5.12 cells cease dividing, the mean cell size decreases and there is a decrease in size variation (Fig. 1A; Fig. 1D). Ki-67 antibody staining declines 35-fold, as assayed by flow cytometry (Fig. 1B). There is also a decrease in RNA content as measured by acridine orange (AO) staining, another reported characteristic of the G0 state (Fig. 1C) (London and McKearn, 1987).

When stimulated by IL-3 FL5.12 cells resume growth and proliferate. We characterized the kinetics of the quiescent-proliferative transition by measuring G1 length and entry into S phase by BrdU-7AAD incorporation and flow cytometry, cell volume by Coulter counter, and the expression of various cell cycle markers by Western blot. S phase begins at 8 – 12 hours for >10% of cells (Fig. 1D). Cell size increases from 350fL to ~550fL as cells go through the first cell cycle (Fig. 1E). There is asynchrony in the cell cycle distribution with time and this is reflected in the broadening of the size distributions. We profiled cyclins and cyclin dependent kinases (Fig. 1F) (Malumbres and Barbacid, 2005; Murray, 2004; Sherr and Roberts, 2004). Cyclin E, begins to increase at 8 hours, consistent with the BrdU measurements, thus denoting the G1/S transition. Cyclin A, cyclin B and Cdk1 increased at 16 – 20h, characteristic of the G2-M phases.

Dynamics of protein expression

Using 6-plex tandem mass tags (TMTs), we measured the relative levels of different proteins at different times during the transition from G0 into the cell cycle (Experimental Procedures) (Ting et al., 2011). In biological duplicate experiments, we quantitated 43,000 unique peptides corresponding to 6,700 unique proteins; >4,700 were common to both experiments (Fig. S1A). The relative expression of each protein was defined to be the average profile of all corresponding peptides from each experiment. Each temporal profile was normalized by its mean value for the purposes of comparison and visualization. 2,666 proteins show well-correlated profiles between the duplicates; these reproducible proteins were the focus for subsequent analysis (Pearson correlation coefficient > 0.5; Datafile S1).

Unsupervised hierarchical clustering of the 2,666 protein abundance changes, using the Euclidean distance as a similarity metric after standardization, showed that duplicate experiments cluster together at each time point and also recaptured the temporal order, suggesting overall gradual changes of protein expression over time (Fig. 2A). The global expression pattern yields two different temporal clusters corresponding to a transition phase from G0 into G1 (0h and 4h) and another clear transition from mid G1 onwards into S phase and mitosis (8h to 20h). There are two main groups of proteins that have opposing expression patterns, where one group is up-regulated in G0/G1 and down-regulated in S/M/G2 and the other main group exhibiting the opposite pattern. For subsequent analysis, we averaged the expression profiles from the duplicate experiments and performed Principal Component Analysis (PCA) to obtain a different global view of the data. The first two principal components (PCs) explained 86.9% of the total variation (Fig. S1B). The first two time points (G0/G1 transition) were clearly distinguished from the remaining time points (Fig. S1B), consistent with the hierarchical clustering analysis. Moreover, the two PCs identified several individual proteins whose expression variations make a major contribution to each PC (Fig. S1B).

To identify individual dynamic proteins, we calculated the maximum fold change (MFC), defined as the ratio of the maximum level to the minimum level for a given expression profile. The mean value of MFCs of 2,666 protein profiles is ~1.53 and the median is ~1.38. There are 240 proteins whose MFCs are greater than 2. The top 2 proteins, Nek6 and Phlda1, have MFC of approximately 29 and 18, respectively. Nek6 is serine/threonine-protein kinase or NimA-related kinase, which plays an important role in mitotic cell cycle progression and is also a cancer therapeutic target (Jeon et al., 2010; Meirelles et al., 2014; Nassirpour et al., 2010). Phlda1, pleckstrin homology-like domain family A member 1, is involved in the apoptotic response (Park et al., 1996; Toyoshima et al., 2004). Nek6 and Phlda1 were increased 15- and 13-fold, respectively, from T = 0h to T = 4h (the highest top 2), suggesting that both mitosis and apoptosis immediately respond to the IL-3 activation for the transition from G0 into the cell cycle.

We identified 16 highly confident proteins where all pairs of peptides have Pearson correlation coefficients of greater than 0.8 and which suggest that the proteomic data mirrors expected cellular responses. Among these are 7 proteins with the maximum fold change (MFC) > 4: Fgl2, Nfil3, Eef2k, Junb, Itm2b, Aen, and Rrn3. Fgl2, Nfil3, Eef2k, Junb, and Rrn3 were among the top targets based on PCA and MFC above. The expression profile of

Nfil3, a transcription factor limited to T cells and related cells, shown in Fig. 2B, demonstrates that the data from the duplicate experiments can be very reliable on the measured peptide level and that the up-regulation in G1 is as expected for a response to the IL-3 activation. Fgl2 (Fibroleukin), with the highest MFC = 9.2, is a 432-amino-acid transmembrane regulator in both innate and adaptive immunity. It has a role in the negative regulation of regulatory T (Treg) cell proliferation and the positive regulation of B cell apoptosis (Shalev et al., 2008). Our data confirm that it should be down-regulated in G0 reflecting suppression of apoptosis due to Bcl-2 and highly up-regulated in response to IL-3 peaking at 4h of early G1 (Fig. 2C). Eef2k is a kinase that is involved in translational inhibition by suppressing a translation elongation factor, Eef2. Junb, which increases about 6 fold on going from G0 to G1, is a transcription factor that is up-regulated in response to growth factors; Itm2b is a broadly expressed membrane protein of unknown function; it continually decreases ~4.5 fold from G0 to G2/M. Aen is an exonuclease downstream of p53 with a role in amplifying apoptotic signals; its abundance is the lowest in G0, increases up to ~4.5-fold in mid-G1 and then decreases in the proliferative state of S/G2/M. Rrn3 is a RNA polymerase I (Pol I)-specific transcription initiation factor for ribosomal DNA (rDNA). The interaction of Rrn3 and Pol I is essential for rDNA transcription and they dissociate upon transcription (Hirschler-Laszkiewicz et al., 2003). Its up-regulation by ~4.4-fold between G0 and G1 is consistent with a growth signal by IL-3 or the increasing abundance of ribosomal proteins. The following down-regulation suggests its dissociation from Pol I upon rDNA transcription as the growth signal diminishes. In Fig. 2D we illustrate 60 proteins that also give highly confident patterns but with smaller MFC and which illustrate the regulation of several cellular processes on entering a proliferative phase: cell cycle, IL-3, B-cell receptor, and PI3K signaling, autophagy, translation initiation, translation elongation, DNA replication, and mitosis.

To obtain more global functional insight we performed functional enrichment analysis by the hypergeometric test using Gene Ontology (GO) terms (Experimental Procedures). The most significant terms with p-value < 0.001 include nucleolus, ribosome, mitochondrion, structural constituents of ribosomes, ATP binding, translation initiation factor activity, translation, and rRNA processing, which are mostly up-regulated on entry to the cell cycle (Fig. S2). This suggests that translation/protein synthesis related proteins play important roles during the proliferative transition of quiescent FL5.12 cells in response to IL-3, in agreement with a previous study on T-cell activation entering the first cell cycle (Orr et al., 2012).

Dynamics of protein modules

We can produce a narrative for one protein at a time that is useful in validating our general study of physiological regulation on entering the cell cycle. However, such tedious narrative building fails when dealing with poorly characterized proteins or with proteins where there was no clear expectation of behavior. To consider the problem in a more objective fashion we analyzed the proteomic results in terms of functionally related protein groups or modules, which includes but is not limited to physical protein complexes. First, based on our previous efforts in other species (Vinayagam et al., 2013), we built a large repository of mouse protein modules by systematically compiling known and predicted modules

(Experimental Procedures). We then applied the COMPLEAT tool (Vinayagam et al., 2013) to analyze our proteomic TMT data and to generate temporal expression profiles of modules (Experimental Procedures). We identified significantly enriched modules based on module scores and p-values (Experimental Procedures). An example of a module, the condensin complex, and its abundance profile is shown in Fig. 3A.

We prioritized dynamically regulated modules using multiple filtering criteria (Fig. 3B to 3E and Experimental Procedures). This yielded a final list of 821 dynamic modules with 311 of them literature-supported (Fig. 3E; Datafile S1). We found that 10–15% of all protein modules from the literature are dynamic during the transition from G0 to the first cell cycle. Unsupervised hierarchical clustering of the 311 literature-supported modules clearly distinguishes the G0/G1 transition from the cell cycle (Fig. S3A). Thus the behavior of these literature-supported dynamic modules show behavior consistent with proteomic changes discussed above (Fig. 2A).

To search for other characteristic dynamic features during the cell cycle we identified modules whose scores peaked at each time point. The G0 state had the highest fraction of 32% (Fig. 3F). The peak modules from 4h to 20h in Fig. 3F include physical complexes functioning in: IL-3 signaling (4h), transcription initiation (8h), ribosome biogenesis (12h), DNA replication (16h), and mitosis (20h). The module at 0h, the citrate cycle, is a group of functionally related enzymes to which we pay particular attention in the next section. As a means to further functionally support the identified modules, we also built a global functional map of the 311 dynamic modules by organizing them using the Gene Ontology (GO) enrichment (Fig. S3B). From this map we could manually identify 77 unique modules, as confidence builders, functioning in 15 biological processes from which we can expect certain expression patterns (Fig. S3B).

The cell cycle entry from G0 shares several of the hallmarks of cancer metabolism

From our global functional map of protein modules, we paid a particular attention to the TriCarboxylicAcid cycle (TCA cycle) because all 4 modules show significant coherence of expression including the module of citrate cycle (Fig. 3F), also referred to as second carbon oxidation (MC2490). Cancer cells, a prototype for proliferative cells (Vander Heiden et al., 2009), repress mitochondrial metabolism in favor of ATP generation through glycolysis. The observed down-regulation of 4 TCA modules suggests that FL5.12 cells behave similarly as they exit the resting state and enter the cell cycle. This observation drove us to look at other metabolic pathways related to cancer as well as individual metabolic enzymes. We examined closely 8 metabolic pathways: the TCA cycle, glycolysis, de novo pyrimidine biosynthesis, de novo purine biosynthesis, pyrimidine salvage, purine degradation, lipid synthesis, and the urea cycle (Figs. 4 – 5 and S4A – S4H). The urea cycle was included in this list of biosynthetic pathways because it has ties to nitrogen and nucleotide metabolism and was shown to be down-regulated in some cancer cells (Feun et al., 2008; Phillips et al., 2013).

We detected all the TCA cycle enzymes, as well as the pyruvate dehydrogenase (PDH) complex (Pdhb, Pdha1, and Pdhx; see Fig. 4A). Collectively, their temporal profiles show consistent and statistically significant down-regulation during the proliferative transition ($p < 0.004$; Fig. 4B and Table S1). Note that Pdk1/2/3, the kinase family that inhibits the PDH

complex in the entry to the TCA cycle, is up-regulated (Peters, 2003). The down-regulation of the TCA cycle is also supported by an overall down-regulation of component proteins of the electron transport chain (ETC) complexes (Fig. S4I). In contrast, the behavior in glycolysis is just the opposite (Figs. 4C and S4B). Txnip, the inhibitor of glucose transport, is down-regulated and Slc2a1 (Glut1), the glucose transporter, is up-regulated during the G0/G1 transition.

This was previously observed (Wu et al., 2013) and confirmed by Western blotting in our study (Fig. 4C). The activation of glucose uptake is among the best-characterized features of cancer metabolism (Bauer et al., 2004; Ying et al., 2012; Yun et al., 2009). Moreover, all the ATP generating and rate-limiting enzymes in glycolysis – Hk2/3, Pfkl, Pfkm, Pfkp, and Pkm2 – and Eno3 are also up-regulated upon the transition into the cell cycle, suggesting that the activation of glycolysis in this context is a highly coordinated process.

All enzymes in the pyrimidine and purine de novo biosynthetic pathways (Figs. S4C and S4D), are up-regulated during G0/G1 transition, as expected for cell growth and proliferation. Some anabolic enzymes in nucleotide biosynthesis, including rate-limiting enzymes, such as Cad, Gart, Adsl, Adss, and Impdh1/2 increase in G1 and reach maximal levels after the S phase. The up-regulation of each enzyme group is statistically significant (p-value < 0.04; Table S1). In the pyrimidine salvage pathway (Fig. S4E), Uprt and Uck2, which convert uracil, uridine, and cytidine to UMP and CMP, are also up-regulated during the G1 phase and then down-regulated thereafter. On the other hand, Cmpk1, Entpd3, and Nme3, which regulate uridine phosphate levels, are down-regulated. In the purine degradation pathway (Fig. S4F), most enzymes are down-regulated. The coordinated up- and down-regulation of the biosynthesis and salvage pathways, respectively, illustrates how the cells regulate the generation of new nucleotides for genome duplication. Acetyl-CoA carboxylase 1 (Acaca), the rate limiting enzyme in fatty acid synthesis that converts acetyl-CoA to malonyl-CoA, Fatty acid synthase (Fasn), and HMG-CoA synthase (Hmgcs1) are up-regulated in the G1 phase and would seem to accelerate lipid biosynthesis, presumably to support biomass generation. In addition, we find that a cytoplasmic fatty acid binding protein, Fabp5, is up-regulated in the proliferative state of G1 to S (Fig. S4G). Fabp5 has been shown to be highly up-regulated in human breast cancers and is a prognostic marker and a potential therapeutic target (Levi et al., 2013; Liu et al., 2011).

The canonical urea cycle consists of 5 enzymes but not all 5 enzymes are necessarily expressed in all cell or tissue types (Morris, 2002). We detected 3 enzymes: carbamoyl phosphate synthase 1 (Cps1), argininosuccinate synthase (Ass1), and argininosuccinate lyase (Asl), which are all down-regulated upon IL-3 activation (Fig. S4H). In particular, the rate-limiting enzyme, Cps1, exhibits a dramatic 4.8-fold decrease in its abundance during the first 4 hours of the G0/G1 transition. The down-regulation of the urea cycle presumably favors the use of nitrogen for biosynthetic purposes of cell growth, over the excretion of urea. The down-regulation of the 3 enzymes as a group is statistically significant (p-value < 0.02; Table S1).

Correlation of metabolite levels with enzymes

We were interested in whether the very clear changes in metabolic enzymes were reflected in their metabolites. Using a general metabolomics platform (Yuan et al., 2012), we detected 291 metabolites at the 6 time points in biological triplicates and obtained a filtered list of 155 metabolites for subsequent analysis (Experimental Procedures; Datafile S1). Unsupervised hierarchical clustering revealed that the data are reproducible and that the metabolomic profiles are similar between neighboring time points (Figs. S5A and S5B). However, unlike the global proteomic changes that show significant changes at the G0/G1 transition (Fig. 2A), the global metabolomic changes are seen as cells begin to enter S phase (T = 12h onwards). 106 metabolites show coefficients of variation (CVs) less than 0.4 at all time points, which we consider as confidently measured.

In order to make a comparison between protein enzymes and metabolites, we mapped all confidently measured metabolites to the 8 metabolic pathways discussed above. The vast majority of enzymes show consistent patterns but this is much less true for their metabolites. The fluctuation of metabolites is also greater than that of enzyme levels (MFC = 7.2 vs. 4.3, respectively). Enzymes that are consistently down-regulated in the TCA cycle, showed variable metabolite patterns (Figs. 4A and 4B). Some metabolites such as citrate, isocitrate, alpha-ketoglutarate, fumarate, and malate are up-regulated during the G0–G1 transition. In glycolysis (Fig. S4B), the proteomics data showed that the abundance of the glucose transporter (Glut1) increases and that the profiles of rate limiting enzymes such as Hk2/3, Pfkl/m/p, and Pkm2 are suggestive of increased glycolytic flux. This is not altogether surprising as we would expect to have seen greater correlations of enzyme level with metabolite flux, since enzymes would increase the rate of the reactions.

A closer correlation between enzymes and their metabolites can be found in pathways other than sugar metabolism. In the de novo pyrimidine biosynthesis pathway (Fig. S4C), the enzymes are up-regulated, presumably in response to the increased demand for nucleotides during cell growth and proliferation. The final product, UMP, is up-regulated as the cells pass through the cell cycle, while dihydroorotate is consumed as expected for pyrimidine synthesis during cell growth. Similar trends are observed for the purine de novo pathway (Fig. S4D). The 12 enzymes and the end products, AMP and GMP, are consistently up-regulated after entry into the cell cycle. In the pyrimidine salvage pathway (Fig. S4E), the anabolic enzymes, Uprt and Uck2, are up-regulated during G1, while the catabolic enzymes, Cmpk1, Nme3, and Entpd3, are down-regulated, as expected. Correspondingly, the upstream metabolites, uracil, uridine, and cytidine, are down-regulated and the downstream metabolites, UMP, UDP, UTP, CMP, CDP, and CTP, are up-regulated over time. In the purine degradation pathway (Fig. S4F), the enzymes are down-regulated and the metabolites show a sharp decrease in their abundance during the G0/G1 transition. This implies that the degradation pathway is not activated, favoring purine synthesis for cell growth. The 8 metabolites detected in this pathway are down-regulated in a statistically significant fashion (p-value < 0.003; Table S1). In the urea cycle (Fig. S4H) carbamoyl phosphate levels exhibit a large gradual decrease (MFC = 5.4), presumably reflecting the major down-regulation of Cps1. This may also be related to increased pyrimidine synthesis, which consumes

carbamoyl phosphate. We also observe corresponding decreases of ornithine and urea, possibly reflecting the use of free nitrogen for biosynthetic purposes.

Despite some expected correlations, the changes in the relative abundance of enzymes and metabolites are not easily explained. To search for explanations, we looked for correlations between enzymes and metabolites in each pathway. We first obtained average enzyme and metabolite time profiles (Fig. 5A). The TCA cycle, glycolysis, and lipid synthesis showed no obvious correlations between enzyme and the corresponding metabolite levels while other pathways show either positive or negative correlations. To better quantify these relationships, we calculated absolute Pearson correlation coefficients for all pairs between enzyme abundance profiles and metabolite abundance profiles and their mean value in each of the seven metabolic pathways, excluding lipid synthesis in which only 1 metabolite (citrate) was measured. For each pathway, we performed a statistical significance test for the mean value by random sampling of enzymes and metabolites (Experimental Procedures). The correlations between enzyme and metabolite profiles are overall better than expected by chance (p-value < 0.09) except for the TCA cycle and glycolysis (p-value > 0.4) (Fig. 5A). This was expected due to large variation in metabolite abundance considered above. The most likely explanation is that metabolites in these pathways are also acted on by enzymes in other pathways, which have their own dynamics (Ward and Thompson, 2012). In contrast, metabolites in nucleotide metabolism are more restricted to their specific pathways and, as such, exhibit correlations.

We also looked for cross correlations between enzyme profiles in one pathway and metabolite profiles in another pathway to understand inter-relationships. This modular cross-correlation analysis generated an asymmetric correlation matrix of the 8 pathways (Fig. 5B). The enzymes in the TCA were strongly correlated to the metabolites in the urea cycle but those enzymes were negatively correlated with metabolites in glycolysis and TCA. The enzymes in those cycles were negatively correlated with TCA metabolites and glycolysis metabolites. The metabolites in glycolysis and the TCA cycle are positively correlated with the enzymes in the pyrimidine and purine de novo pathways, while they are negatively correlated with the enzymes in the purine degradation and the pyrimidine salvage pathway. For a further global insight, we paid a particular attention to those cross correlations that are better than either of the two within-pathway correlations. As shown in Fig. 5C, the enzyme profiles in glycolysis have higher correlations with the metabolite profiles in all the other 6 pathways than those in glycolysis itself. This again supports the fact that glycolytic intermediates are used as precursors for several other metabolic pathways, among which are nucleotide and amino acid biosynthetic pathways. On the other hand, the measured enzymes in nucleotide metabolism and the urea cycle do not show such high cross correlations, implying that those enzymes are specific to their pathways. We conclude that metabolite dynamics show more complex patterns than enzyme dynamics and that nucleotide metabolism is a more specialized process than others showing correlated dynamics between enzymes and metabolites.

Extracellular metabolite profiling underscores proliferative metabolic changes

Another very useful perspective of metabolic changes is revealed in how metabolites are consumed from and released into the growth medium. The metabolite levels in the control fresh media were used as a reference for all time points. Unsupervised hierarchical clustering again revealed that the data are reproducible and that the neighboring time points have similar profiles, except for T = 0h (Fig. S5C). It is reasonable that the abundance levels of extracellular metabolites in the media at T = 0h, which is the G0 state after the 36-hour IL-3 deprivation, are similar to those at T = 16h and 20h rather than T = 4h, in accordance with longer consumption of/exposure to the extracellular media. By dividing by the control media metabolite levels, we obtained a final list of 173 normalized metabolite levels for all time points (Fig. S5D; Datafile 1). As a measure of the dynamic range of abundance levels, we calculated MFC as above. There are 44 metabolites whose MFC is greater than 4, among which 11 metabolites have MFC greater than 10. The top two dynamic metabolites are lysine (Lys) and methionine (Met), which showed MFC > 110 and MFC > 50, respectively. Both metabolites were consumed from the media by the cells, especially at the G0 and S/G2/M phases. Three other amino acids – phenylalanine (Phe), valine (Val) and tryptophan (Trp) – show a similar pattern of rapid consumption over time, meaning that they were depleted from the media as the cells entered the S phase.

Extracellular levels of pyruvate and lactate increased during the first cell cycle (Fig. 6A), which provides clear support for up-regulation of glycolysis during the proliferative transition and functionally validating the proteomics data above (Fig. 4B). Interestingly, we also observed that lactate in the media was consumed by the cells in G0. This likely reflects an effort by these cells to obtain and utilize non-glucose carbon sources since glucose uptake is down-regulated through Txnip-dependent repression of glucose transporter expression in G0, as discussed above.

Amino acid consumption as a function of the cell cycle

The proliferative transition accompanies up-regulation of translation and ribosome biogenesis (Figs. 2D, 3F, S2 and S3B), suggesting correlated changes in amino acid uptake, biosynthesis and utilization. To quantify amino acid consumption, we converted the normalized relative values into absolute concentrations at each time point based on the media formulation (Experimental Procedures; Fig. S6A). The initial amino acid concentrations vary significantly from as high as 1.15mM (Arg) to 24.5μM (Trp). Perhaps among the most interesting observations was the correlation between uptake and excretion among essential amino acids (EAA) and non-essential amino acids (NEAA; Fig. 6B). Like αKG, Glu was released from cells (0.39mM in G0 and 0.16 – 0.37mM in the first cell cycle; Fig. S6A) suggesting a large role for Gln in nucleotide biosynthesis and the release of Glu. Studies in cancer cell lines support this interpretation (Jain et al., 2012; Marin-Valencia et al., 2012). We also observe that the resting population (36 hours without IL-3) and the proliferating population in the late G1 phase (8h – 12h) consumed amino acids to a similar degree.

Focusing on the nine measured EAAs, we calculated the difference in amino acid consumption at two adjacent times to obtain the consumption rate in 4-hour intervals. In

addition, we used the relative frequency of EAA abundance in proteins to normalize uptake of a specific EAA to the rate of protein synthesis, assuming no other potential functions of these amino acids. For this purpose, we used the evolutionarily observed frequencies from a previous study (King and Jukes, 1969), which turns out to remain relatively constant regardless of the biological context (Fig. S6B). The normalized consumption plot revealed that Met (whose observed frequency in proteins is 1.8%) was consumed more than the other 8 measured EAAs (whose average frequency in proteins is 4.9%) by about 2-fold during the late-G1 to S phase (8h – 16h; Figs. 6C and S6C – S6E). Met and the average of the other EAAs were consumed most during the late G1 and S phases (8h – 12h), the peak time when protein synthesis occurs. However, Met was consumed more at the G1-S phase (8h – 12h) than at the G0–G1 phase (0h – 4h) by about 12-fold, compared to 5.6-fold on average for the other amino acids. Met consumption becomes even higher than the other EAAs by about 4-fold if we exclude the conditional amino acid, Arg, whose consumption is highest at the early G1 phase (4h – 8h; Figs. S6D – S6E). The early response of Arg uptake to IL-3 activation is supported by the fact that the arginine metabolism is related to downstream production of metabolites such as nitric oxide and polyamines that have an important role in cell growth and proliferation (Peranzoni et al., 2007; Satriano, 2004).

Met constitutes the primary metabolic input for S-adenosyl-methionine (SAM) biosynthesis. SAM is the cofactor for methyl transfer reactions required to establish the epigenetic methyl marks on nascent DNA and histones (DNA and histone methylation) (Shyh-Chang et al., 2013; Varela-Rey et al., 2014). The peak consumption of Met (G1-S phase) closely tracks with the observed patterns in nucleotide biosynthesis, providing a rationale for both its relative increased rate of consumption and the cell cycle position at which this occurs. Furthermore, a pathway analysis of metabolites whose MFC > 4 shows that two downstream metabolites, SAM and S-methyl-5-thioadenosine, exhibit intracellular abundance patterns that track 4 hours behind that of Met (Fig. S6F). The importance of Met metabolism was also supported by the protein expression profile of Dnmt1, the major DNA methyltransferase for CpG cytosines to maintain the methylation pattern during replication (Fig. 2D), which peaks during the S phase following high Met consumption during G1. There is also elevated expression of other Met-consuming epigenetic enzymes, including methionine synthase, Mtr, peaking at T = 12h (G1-S phase), S-adenosylmethionine synthetase isoform type-2, Mat2a, peaking at T = 8h (mid-late G1 phase), lysine methyltransferase, Smyd2, peaking at T = 12h, and arginine methyltransferase, Prmt7, peaking at T = 12h, with MFC between 1.4 and 3.8 (Fig. 6D). Moreover, 1-methylnicotinamide (1MNA), which was recently reported to play a role as a methylation sink after obtaining the methyl group from SAM in the Met cycle in tumor cells (Ulanovskaya et al., 2013; Ye et al., 2017), is highly secreted in our system with more than 16-fold increase in the media from T = 12h on (Fig. 6D). The abundance of its precursor metabolite, nicotinamide, in the media is reduced as well as its intracellular abundance, as expected (Fig. 6D). We further correlated Met consumption with the levels of 5 histone tri-methylation marks: H3K4me3, H3K9me3, K3K27me3, H3K36me3, and H3K79me3 (Fig. 6E). The peaks of intracellular Met and SAM at 4h and 8h overlap with the peaks of the 5 tri-methylated histones at 12h, suggesting Met was also consumed for histone methylation through SAM.

DISCUSSION

Our model system of FL5.12 cells in response to IL-3 is perhaps a superior model for the G0/G1 transition to the more common serum-starvation and refeeding experiments that carry with them the complexity of signals in serum and the concerns of synchronization and re-activation (Cooper and Gonzalez-Hernandez, 2009). While there still exists a significant fraction of cells that loses synchrony in our system along the cell cycle, a significant sub-population of cells remarkably gave rise to major known characteristics and features of each cell cycle phase as evidenced in Figs. 1F and 2D. Therefore, our study improves a molecular understanding of cell cycle in a more quantitative way despite potential limitations and caveats regarding intrinsically incomplete synchrony in our system such as difficult interpretations of metabolite abundance profiles discussed below.

Dynamicity of the functional protein modules registered unambiguously in our proteomic measurements. Enzyme abundance profiles revealed many aspects of cellular metabolism whose regulation by the cell cycle has previously not been as well appreciated. The metabolite profiling was more difficult to interpret. Whereas the proteomic data registers the enzyme levels, which would be expected to correlate with the flux through the pathways, steady state metabolite concentrations can take high or low values under conditions of high flux. For such reasons, steady state metabolite levels are hard to relate to enzyme levels. In addition, numerous metabolites in central carbon metabolism can be substrates/products of multiple reactions in independent pathways, which can confuse any analysis based solely on the enzyme concentrations of the core pathways. Experimental measurement of flux using labeled substrates would help clarify these issues as well as using better-synchronized cell populations.

The changes of metabolic state in the G0–G1 transition in the pro-B lymphocyte line invite a comparison to cancer. Although there have been several studies of gene expression, proteomics, and metabolism in proliferation and quiescence (Coloff et al., 2016; Lemons et al., 2010; Valcourt et al., 2012; Venezia et al., 2004), a quantitative description of the proteome of G0 cells and their transition into the cell cycle has been generally lacking. Our proteomic survey shows that they are remarkably similar to recent studies of the G1 state in the cancer metabolism literature, where the cells are in a constant proliferative state (Munoz-Pinedo et al., 2012; Schulze and Harris, 2012; Wheatley, 2005).

The metabolic profiling of extracellular metabolites revealed that Met consumption dramatically increases during the G1 phase compared to other EAAs. This would not be expected if all EAAs including Met were consumed only for protein synthesis. In that case the amount of each EAA should reflect its relative abundance in the proteome. A similar observation was made for L-arginine in a recent proteomics and metabolomics study of activated human naïve T cells (Geiger et al., 2016). An explanation for the high consumption of Met might be that it has additional functions, such as a source of methyl groups for protein methylation including epigenetic marks (Waterland, 2006). Alternatively, highly proliferative cells could drain methyl groups from the Met cycle into 1-methylnicotinamide (1MNA), decreasing histone/protein methylation (Ulanovskaya et al., 2013). Both appear to happen. We find that extra-cellular nicotinamide and 1MNA are anti-correlated with

intracellular nicotinamide and 1MNA (Fig. 6D), which could lead to a decrease of histone/protein methylation, despite higher Met intake. However, the proteomics data also support increased intracellular Met use. 5-methyltetrahydrofolate-homocysteine methyltransferase (Mtr), an enzyme involved in Met synthesis, peaked at G1-S (Fig. 6D) and the major DNA methyltransferase for replication, Dnmt1, as well as its interacting protein, Dmap1, for transcriptional repression, are up-regulated during S phase (Rountree et al., 2000) (Fig. 2D). These 3 up-regulated proteins have each been investigated as therapeutic targets in cancer (Cheray et al., 2013; Tang et al., 2008). We also observed several other up-regulated methyltransferases such as Dot1l, Prmt3/5/7, Smyd2, Ezh2, Dnmt3b (Figs. 6D and S7A). On the other hand, we observe diverse patterns of 7 histone demethylases: Kdm1, Kdm3a, Kdm3b, Kdm4a, Kdm5b, Kdm5c, and Kdm6b (Fig. S7B). Although we cannot attribute histone specificity of the individual methylating enzymes, the 5 histone trimethylation marks showed a temporal correlation with the levels of Met and SAM in their peak abundance levels (Fig. 6E). A recent study also showed that histones could serve as a methylation sink (Ye et al., 2017), in addition to 1MNA. Moreover, the up-regulation of Met and SAM from the mid-G1 phase is correlated with the down-regulation of the two protein modules, SIRT1-LSD1 complex (MC289) and CtBP core complex (MC1067), which have roles in histone demethylation to repress target genes (DNA methylation in Fig. S3B). We also note that homocysteine, a metabolite in the Met cycle, shows an opposite regulation pattern to Met and that the up-regulation of homocysteine is accompanied by down-regulation of glutathione peroxidase 1, Gpx1, a situation found in hyperhomocysteinemia (Fig. S7C) (Handy et al., 2005). This suggests an additional demand for Met, which contributes to the interpretation of Met levels. The importance of Met and SAM for growth seems indisputable; a recent study reported that depletion of either Met or SAM induced G1 cell cycle arrest in FL5.12 and its derivative cells (Lin et al., 2014).

The metabolomic and related proteomic map of IL-3 activation is summarized in Fig. 7. It bears strong resemblance to features attributed to cancer cells. Based on our results outlined in this model, we suggest that IL-3 mediated activation of the cell cycle is similar to cancer in several important ways as follows and shed light on cancer metabolism. Modules and proteins that are highly abundant in G0 are then abundant again from the S phase onwards (Fig. 7A, purple and blue bars of “modules” and “proteins”, respectively). These changes offer clues about how cancer cells may adapt in nutrient-deprived states (G0), and how they progress after tumorigenic transformation (S phase onwards). Dynamic changes in intracellular metabolite levels are evident in G0, early G1, S, and G2/M phases (MFC > 2.49; Fig. 7A, yellow bars of “intra”). These results suggest that metabolic activity is most evident during these stages of the cell cycle. These cells are the most avid for extracellular nutrients (i.e. uptake) in early G1, S and G2/M phases (Fig. 7A, green bars of “extra in”). On the other hand, metabolite release occurs mostly in G0 and G2/M phases (Fig. 7A, red bars of “extra out”). These results parallel the catabolic (nutrient breakdown for energy) versus anabolic (nutrient capture for biosynthesis) phases of the cell cycle. Based on this, we can hypothesize a potential relationship between our model and cancer studies: cancer adaptation occurs in G0 (e.g., Eef2k and Eif4e3), oncogenic transformation in G0/G1 (e.g. Nek6 and Phlda1), and cancer progression during the first cell cycle (e.g. Rrm2). Among cancer types, our study will be immediately relevant as a tool to understand underlying

molecular mechanisms of acute myeloid leukemias (AMLs), which possess abnormalities of the IL-3 receptor alpha chain, IL-3Ra or CD123 (Munoz et al., 2001; Steelman et al., 2004; Testa et al., 2014; Testa et al., 2004).

A major question in the field of cancer metabolism concerns how to target metabolic features of cancer cells that are often shared with normal proliferative and/or stem cells (Vander Heiden, 2011). Given that many of the metabolic characteristics of the proliferative transition in our system are seen in cancers, our findings can be explored carefully for therapeutic windows based on cancer metabolism. Furthermore, we also expect that our system provides insight into cancer metabolism directly and how its dysregulation can be used to select metabolic enzyme targets, pathways and networks (Zhao et al., 2013). In particular, nucleotide-metabolism-targeted chemotherapies have high associated toxicities because this is a feature shared with normal proliferative cells.

EXPERIMENTAL PROCEDURES

Experimental Model

A murine pro-B lymphocyte cell line, FL5.12-Bcl-2, was a gift from Dr. Anthony Letai at Dana Farber Cancer Institute. The cells were cultured in RPMI 1640 (Invitrogen) supplemented with 10% calf bovine serum (ATCC, catalog #30-2030), 1% 100× penicillin/streptomycin (Gemini), 1% Geneticin (Invitrogen, catalog #10131-035), and 50mM 2-mercaptoethanol (Sigma/Aldrich), and 3ng/ml IL-3 (R&D Systems, catalog #403-ML-010). For the G0 synchronization, the cycling cells were washed 3 times with warm PBS and then cultured in the same media excluding IL-3 for 36 hours. For activation, the quiescent cells were re-suspended in the complete media including IL-3.

Cellular and Molecular Assays

Cell number counting, cell size measurement, acridine orange assay, BrdU assay, and Western blotting are described in Supplemental Experimental Procedures.

Tandem Mass Tags (TMT)-Mass Spectrometry Proteomics

For details, see Supplemental Experimental Procedures.

LC-MS/MS Targeted Mass Spectrometry Metabolomics

For details, see Supplemental Experimental Procedures.

Bioinformatic and Statistical Analysis

Quantification of abundance levels of proteomics, metabolomics, and protein modules was detailed in Supplemental Experimental Procedures. In general, p-values less than 0.05 were considered significant.

Data and Software Availability

The proteomics, metabolomics, and protein modules profiling data processed in this study are available in the spreadsheet file with this article online (Datafile S1). All software is freely available and listed in the Resource Table.

SUPPLEMENTAL INFORMATION

Supplemental Information includes Supplemental Experimental Procedures, 7 figures, and 2 tables and can be found with this article online.

Supplementary Material

Refer to Web version on PubMed Central for supplementary material.

Acknowledgments

We would like to thank the Kirschner lab members, Tim Mitchison, Joseph Loscalzo, Selina Chen-Kian, Zoltan Maliga, and the anonymous reviewer for their valuable comments and suggestions. This work was supported by the grant #GM26985 to MWK and R01 #GM041890 to LCC. LCC owns equity in, receives compensation from, and serves on the Board of Directors and Scientific Advisory Board of Agios Pharmaceuticals. Agios Pharmaceuticals is identifying metabolic pathways of cancer cells and developing drugs to inhibit such enzymes to disrupt tumor cell growth and survival.

References

Bauer DE, Harris MH, Plas DR, Lum JJ, Hammerman PS, Rathmell JC, Riley JL, Thompson CB. Cytokine stimulation of aerobic glycolysis in hematopoietic cells exceeds proliferative demand. FASEB journal : official publication of the Federation of American Societies for Experimental Biology. 2004; 18:1303–1305. [PubMed: 15180958]

Cheray M, Pacaud R, Nadaradjane A, Vallette FM, Cartron PF. Specific inhibition of one DNMT1-including complex influences tumor initiation and progression. Clinical epigenetics. 2013; 5:9. [PubMed: 23809695]

Coloff JL, Murphy JP, Braun CR, Harris IS, Shelton LM, Kami K, Gygi SP, Selfors LM, Brugge JS. Differential Glutamate Metabolism in Proliferating and Quiescent Mammary Epithelial Cells. Cell Metab. 2016; 23:867–880. [PubMed: 27133130]

Conlon I, Raff M. Size Control in Animal Development. Cell. 1999; 96:235–244. [PubMed: 9988218]

Cooper S, Gonzalez-Hernandez M. Experimental reconsideration of the utility of serum starvation as a method for synchronizing mammalian cells. Cell biology international. 2009; 33:71–77. [PubMed: 18948216]

Feun L, You M, Wu CJ, Kuo MT, Wangpaichitr M, Spector S, Savaraj N. Arginine deprivation as a targeted therapy for cancer. Curr Pharm Des. 2008; 14:1049–1057. [PubMed: 18473854]

Geiger R, Rieckmann JC, Wolf T, Basso C, Feng Y, Fuhrer T, Kogadeeva M, Picotti P, Meissner F, Mann M, et al. L-Arginine Modulates T Cell Metabolism and Enhances Survival and Anti-tumor Activity. Cell. 2016; 167:829–842.e813. [PubMed: 27745970]

Handy DE, Zhang Y, Loscalzo J. Homocysteine down-regulates cellular glutathione peroxidase (GPx1) by decreasing translation. The Journal of biological chemistry. 2005; 280:15518–15525. [PubMed: 15734734]

Hirschler-Laszkiewicz I, Cavanaugh AH, Mirza A, Lun M, Hu Q, Smink T, Rothblum LI. Rrn3 becomes inactivated in the process of ribosomal DNA transcription. The Journal of biological chemistry. 2003; 278:18953–18959. [PubMed: 12646563]

Jain M, Nilsson R, Sharma S, Madhusudhan N, Kitami T, Souza AL, Kafri R, Kirschner MW, Clish CB, Mootha VK. Metabolite profiling identifies a key role for glycine in rapid cancer cell proliferation. Science. 2012; 336:1040–1044. [PubMed: 22628656]

Jeon YJ, Lee KY, Cho YY, Pugliese A, Kim HG, Jeong CH, Bode AM, Dong Z. Role of NEK6 in tumor promoter-induced transformation in JB6 C141 mouse skin epidermal cells. The Journal of biological chemistry. 2010; 285:28126–28133. [PubMed: 20595392]

King JL, Jukes TH. Non-Darwinian Evolution. Science. 1969; 164:788–798. [PubMed: 5767777]

Lemons JM, Feng XJ, Bennett BD, Legesse-Miller A, Johnson EL, Raitman I, Pollina EA, Rabitz HA, Rabinowitz JD, Coller HA. Quiescent fibroblasts exhibit high metabolic activity. PLoS biology. 2010; 8:e1000514. [PubMed: 21049082]

Levi L, Lobo G, Doud MK, von Lintig J, Seachrist D, Tochtrop GP, Noy N. Genetic ablation of the fatty acid-binding protein FABP5 suppresses HER2-induced mammary tumorigenesis. Cancer research. 2013; 73:4770–4780. [PubMed: 23722546]

Lin DW, Chung BP, Kaiser P. S-adenosylmethionine limitation induces p38 mitogen-activated protein kinase and triggers cell cycle arrest in G1. Journal of cell science. 2014; 127:50–59. [PubMed: 24155332]

Liu RZ, Graham K, Glubrecht DD, Germain DR, Mackey JR, Godbout R. Association of FABP5 expression with poor survival in triple-negative breast cancer: implication for retinoic acid therapy. The American journal of pathology. 2011; 178:997–1008. [PubMed: 21356353]

London L, McKearn JP. Activation and growth of colony-stimulating factor-dependent cell lines is cell cycle stage dependent. The Journal of experimental medicine. 1987; 166:1419–1435. [PubMed: 3316471]

Malumbres M, Barbacid M. Mammalian cyclin-dependent kinases. Trends in biochemical sciences. 2005; 30:630–641. [PubMed: 16236519]

Marin-Valencia I, Yang C, Mashimo T, Cho S, Baek H, Yang XL, Rajagopalan KN, Maddie M, Vemireddy V, Zhao Z, et al. Analysis of tumor metabolism reveals mitochondrial glucose oxidation in genetically diverse human glioblastomas in the mouse brain in vivo. Cell Metab. 2012; 15:827–837. [PubMed: 22682223]

McKearn JP, McCubrey J, Fagg B. Enrichment of hematopoietic precursor cells and cloning of multipotential B-lymphocyte precursors. Proceedings of the National Academy of Sciences. 1985; 82:7414–7418.

Meirelles GV, Perez AM, de Souza EE, Basei FL, Papa PF, Melo Hanchuk TD, Cardoso VB, Kobarg J. "Stop Ne(c)king around": How interactomics contributes to functionally characterize Nek family kinases. World journal of biological chemistry. 2014; 5:141–160. [PubMed: 24921005]

Morris SM Jr. Regulation of enzymes of the urea cycle and arginine metabolism. Annual review of nutrition. 2002; 22:87–105.

Munoz L, Nomdedeu J, Lopez O, Carnicer M, Bellido M, Aventin A, Brunet S, Sierra J. Interleukin-3 receptor alpha chain (CD123) is widely expressed in hematologic malignancies. Haematologica. 2001; 86:1261–1269. [PubMed: 11726317]

Munoz-Pinedo C, El Mjiyad N, Ricci JE. Cancer metabolism: current perspectives and future directions. Cell death & disease. 2012; 3:e248. [PubMed: 22237205]

Murray AW. Recycling the Cell Cycle: Cyclins Revisited. Cell. 2004; 116:221–234. [PubMed: 14744433]

Nassirpour R, Shao L, Flanagan P, Abrams T, Jallal B, Smeal T, Yin MJ. Nek6 mediates human cancer cell transformation and is a potential cancer therapeutic target. Molecular cancer research : MCR. 2010; 8:717–728. [PubMed: 20407017]

Nuñez G, London L, Hockenbery D, Alexander M, McKearn JP, Korsmeyer SJ. Deregulated Bcl-2 gene expression selectively prolongs survival of growth factor-deprived hemopoietic cell lines. The Journal of Immunology. 1990; 144:3602–3610. [PubMed: 2184193]

Orr SJ, Boutz DR, Wang R, Chronis C, Lea NC, Thayaparan T, Hamilton E, Milewicz H, Blanc E, Mufti GJ, et al. Proteomic and protein interaction network analysis of human T lymphocytes during cell-cycle entry. Molecular systems biology. 2012; 8:573. [PubMed: 22415777]

Pardee AB. G1 Events and Regulation of Cell Proliferation. Science. 1989; 246:603. [PubMed: 2683075]

Park CG, Lee SY, Kandala G, Lee SY, Choi Y. A Novel Gene Product that Couples TCR Signaling to Fas(CD95) Expression in Activation-Induced Cell Death. Immunity. 1996; 4:583–591. [PubMed: 8673705]

Peranzoni E, Marigo I, Dolcetti L, Ugel S, Sonda N, Taschin E, Mantelli B, Bronte V, Zanovello P. Role of arginine metabolism in immunity and immunopathology. Immunobiology. 2007; 212:795–812. [PubMed: 18086380]

Peters SJ. Regulation of PDH activity and isoform expression: diet and exercise. Biochemical Society transactions. 2003; 31:1274–1280. [PubMed: 14641042]

Phillips MM, Sheaff MT, Szlosarek PW. Targeting arginine-dependent cancers with arginine-degrading enzymes: opportunities and challenges. Cancer research and treatment : official journal of Korean Cancer Association. 2013; 45:251–262. [PubMed: 24453997]

Planas-Silva MD, Weinberg RA. The restriction point and control of cell proliferation. Current opinion in cell biology. 1997; 9:768–772. [PubMed: 9425340]

Ron-Harel N, Santos D, Ghergurovich JM, Sage PT, Reddy A, Lovitch SB, Dephoure N, Satterstrom FK, Sheffer M, Spinelli JB, et al. Mitochondrial Biogenesis and Proteome Remodeling Promote One-Carbon Metabolism for T Cell Activation. Cell Metab. 2016; 24:104–117. [PubMed: 27411012]

Rountree MR, Bachman KE, Baylin SB. DNMT1 binds HDAC2 and a new co-repressor, DMAP1, to form a complex at replication foci. Nat Genet. 2000; 25:269–277. [PubMed: 10888872]

Satriano J. Arginine pathways and the inflammatory response: interregulation of nitric oxide and polyamines: review article. Amino acids. 2004; 26:321–329. [PubMed: 15290337]

Schulze A, Harris AL. How cancer metabolism is tuned for proliferation and vulnerable to disruption. Nature. 2012; 491:364–373. [PubMed: 23151579]

Shalev I, Liu H, Koscik C, Bartczak A, Javadi M, Wong KM, Maknojia A, He W, Liu MF, Diao J, et al. Targeted Deletion of fgl2 Leads to Impaired Regulatory T Cell Activity and Development of Autoimmune Glomerulonephritis. The Journal of Immunology. 2008; 180:249–260. [PubMed: 18097026]

Sherr CJ. G1 phase progression: Cycling on cue. Cell. 1994; 79:551–555. [PubMed: 7954821]

Sherr CJ, Roberts JM. Living with or without cyclins and cyclin-dependent kinases. Genes & development. 2004; 18:2699–2711. [PubMed: 15545627]

Shyh-Chang N, Locasale JW, Lyssiotis CA, Zheng Y, Teo RY, Ratanasirintrawoot S, Zhang J, Onder T, Unternaehrer JJ, Zhu H, et al. Influence of threonine metabolism on S-adenosylmethionine and histone methylation. Science. 2013; 339:222–226. [PubMed: 23118012]

Singh SA, Winter D, Kirchner M, Chauhan R, Ahmed S, Ozlu N, Tzur A, Steen JA, Steen H. Co-regulation proteomics reveals substrates and mechanisms of APC/C-dependent degradation. The EMBO journal. 2014; 33:385–399. [PubMed: 24510915]

Steelman LS, Pohnert SC, Shelton JG, Franklin RA, Bertrand FE, McCubrey JA. JAK/STAT, Raf/MEK/ERK, PI3K/Akt and BCR-ABL in cell cycle progression and leukemogenesis. Leukemia. 2004; 18:189–218. [PubMed: 14737178]

Tang C, Zhang Z, Xu B, Li M, Liu J, Cui J. Two newly synthesized 5-methyltetrahydrofolate-like compounds inhibit methionine synthase activity accompanied by cell cycle arrest in G1/S phase and apoptosis in vitro. Anti-cancer drugs. 2008; 19:697–704. [PubMed: 18594211]

Testa U, Pelosi E, Frankel A. CD 123 is a membrane biomarker and a therapeutic target in hematologic malignancies. Biomarker research. 2014; 2:4. [PubMed: 24513123]

Testa U, Riccioni R, Diverio D, Rossini A, Lo Coco F, Peschle C. Interleukin-3 receptor in acute leukemia. Leukemia. 2004; 18:219–226. [PubMed: 14671644]

Thompson A, Schafer J, Kuhn K, Kienle S, Schwarz J, Schmidt G, Neumann T, Johnstone R, Mohammed AK, Hamon C. Tandem mass tags: a novel quantification strategy for comparative analysis of complex protein mixtures by MS/MS. Analytical chemistry. 2003; 75:1895–1904. [PubMed: 12713048]

Ting L, Rad R, Gygi SP, Haas W. MS3 eliminates ratio distortion in isobaric multiplexed quantitative proteomics. Nature methods. 2011; 8:937–940. [PubMed: 21963607]

Toyoshima Y, Karas M, Yakar S, Dupont J, Helman L, LeRoith D. TDAG51 Mediates the Effects of Insulin-like Growth Factor I (IGF-I) on Cell Survival. Journal of Biological Chemistry. 2004; 279:25898–25904. [PubMed: 15037619]

Ulanovskaya OA, Zuhl AM, Cravatt BF. NNMT promotes epigenetic remodeling in cancer by creating a metabolic methylation sink. Nat Chem Biol. 2013; 9:300–306. [PubMed: 23455543]

Valcourt JR, Lemons JM, Haley EM, Kojima M, Demuren OO, Coller HA. Staying alive: metabolic adaptations to quiescence. Cell cycle. 2012; 11:1680–1696. [PubMed: 22510571]

Vander Heiden MG. Targeting cancer metabolism: a therapeutic window opens. Nature reviews Drug discovery. 2011; 10:671–684. [PubMed: 21878982]

Vander Heiden MG, Cantley LC, Thompson CB. Understanding the Warburg effect: the metabolic requirements of cell proliferation. Science. 2009; 324:1029–1033. [PubMed: 19460998]

Varela-Rey M, Iruarrizaga-Lejarreta M, Lozano JJ, Aransay AM, Fernandez AF, Lavin JL, Mosen-Ansorena D, Berdasco M, Turmaine M, Luka Z, et al. S-adenosylmethionine levels regulate the schwann cell DNA methylome. Neuron. 2014; 81:1024–1039. [PubMed: 24607226]

Venezia TA, Merchant AA, Ramos CA, Whitehouse NL, Young AS, Shaw CA, Goodell MA. Molecular signatures of proliferation and quiescence in hematopoietic stem cells. PLoS biology. 2004; 2:e301. [PubMed: 15459755]

Vinayagam A, Hu Y, Kulkarni M, Roesel C, Sopko R, Mohr SE, Perrimon N. Protein complex-based analysis framework for high-throughput data sets. Science signaling. 2013; 6:rs5. [PubMed: 23443684]

Ward PS, Thompson CB. Metabolic reprogramming: a cancer hallmark even warburg did not anticipate. Cancer cell. 2012; 21:297–308. [PubMed: 22439925]

Waterland RA. Assessing the effects of high methionine intake on DNA methylation. The Journal of nutrition. 2006; 136:1706s–1710s. [PubMed: 16702343]

Wheatley DN. Arginine deprivation and metabolomics: important aspects of intermediary metabolism in relation to the differential sensitivity of normal and tumour cells. Seminars in cancer biology. 2005; 15:247–253. [PubMed: 15886013]

Wu N, Zheng B, Shaywitz A, Dagon Y, Tower C, Bellinger G, Shen CH, Wen J, Asara J, McGraw TE, et al. AMPK-dependent degradation of TXNIP upon energy stress leads to enhanced glucose uptake via GLUT1. Molecular cell. 2013; 49:1167–1175. [PubMed: 23453806]

Ye C, Sutter BM, Wang Y, Kuang Z, Tu BP. A Metabolic Function for Phospholipid and Histone Methylation. Molecular cell. 2017; 66:180–193.e188. [PubMed: 28366644]

Ying H, Kimmelman AC, Lyssiotis CA, Hua S, Chu GC, Fletcher-Sananikone E, Locasale JW, Son J, Zhang H, Coloff JL, et al. Oncogenic Kras maintains pancreatic tumors through regulation of anabolic glucose metabolism. Cell. 2012; 149:656–670. [PubMed: 22541435]

Yuan M, Breitkopf SB, Yang X, Asara JM. A positive/negative ion-switching, targeted mass spectrometry-based metabolomics platform for bodily fluids, cells, and fresh and fixed tissue. Nature protocols. 2012; 7:872–881. [PubMed: 22498707]

Yun J, Rago C, Cheong I, Pagliarini R, Angenendt P, Rajagopalan H, Schmidt K, Willson JK, Markowitz S, Zhou S, et al. Glucose deprivation contributes to the development of KRAS pathway mutations in tumor cells. Science. 2009; 325:1555–1559. [PubMed: 19661383]

Zetterberg A. Control of mammalian cell proliferation. Current opinion in cell biology. 1990; 2:296–300. [PubMed: 2194528]

Zetterberg A, Larsson O, Wiman KG. What is the restriction point? Current opinion in cell biology. 1995; 7:835–842. [PubMed: 8608014]

Zhao Y, Butler EB, Tan M. Targeting cellular metabolism to improve cancer therapeutics. Cell death & disease. 2013; 4:e532. [PubMed: 23470539]

HIGHLIGHTS

- Proteomic and metabolomic temporal profiling from G0 to cell cycle in response to IL-3
- Global similarities in metabolic reprogramming with cancer cells
- Nucleotide metabolism is highly specialized during the proliferative transition
- Rapid consumption of methionine in G1 serving multiple functions

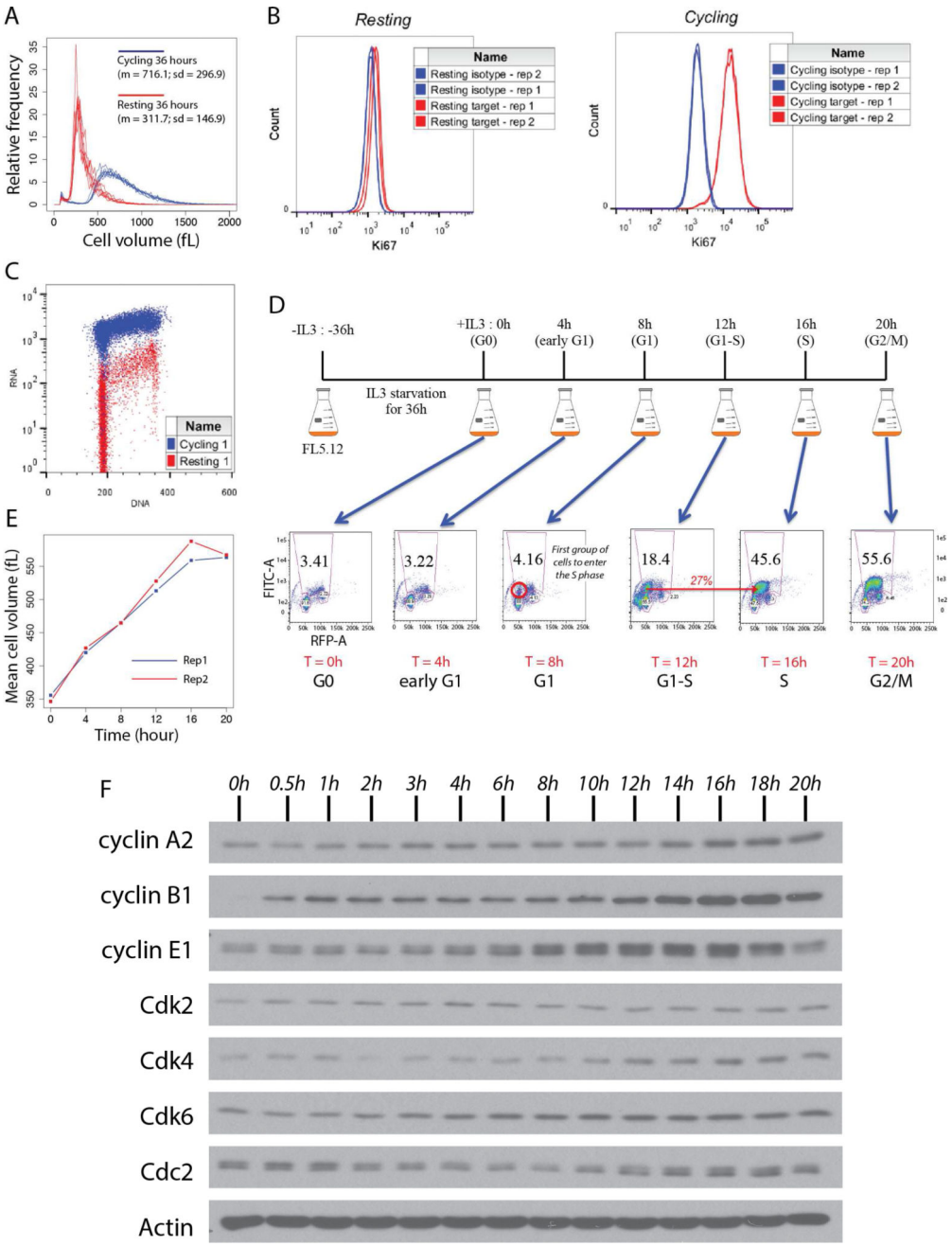

Figure 1. The murine pro-B lymphocyte cell line, FL5.12, exclusively depends on IL-3 for growth and proliferation

We synchronized cells at a quiescence/resting state or G0 by growing in media without IL-3 for 36 hours and then released them from G0 into the cell cycle by re-growing them in the presence of IL-3. (A) Cell size distributions of cycling cells in the presence of IL-3 and resting (or G0) cells in the absence of IL-3 for 36 hours with 7 replicates measured using a Coulter counter. (B) The proliferation marker, Ki-67, shows that FL5.12 cells in G0 do not express Ki-67 and that the cycling cells sampled at 36 hours express Ki-67. (C) An acridine orange (AO) assay distinguishes the resting G0 population from the cycling population by the RNA content. The IL-3-deprived G0 cells have lower RNA content than the cycling

population. (D) A 30-min incubation with BrdU shows how the FL5.12 cells progress into the cell cycle from G0 upon IL-3 stimulation. Samples were collected every 4 hours over the 20 hours of this study. The G1/S transition occurred between 12 hours and 16 hours for the majority of cells. (E) Cell size changes after IL-3 stimulation in duplicates. (F) Western blotting analysis of 7 cell cycle markers: cyclins A2/B1/E1, Cdk2/4/6, and Cdc2 (a.k.a. Cdk1). Actin was used as a control. The G1/S transition can be seen at around 10h from cyclin E; G2/M phases from cyclins A2/B1 and Cdc2.

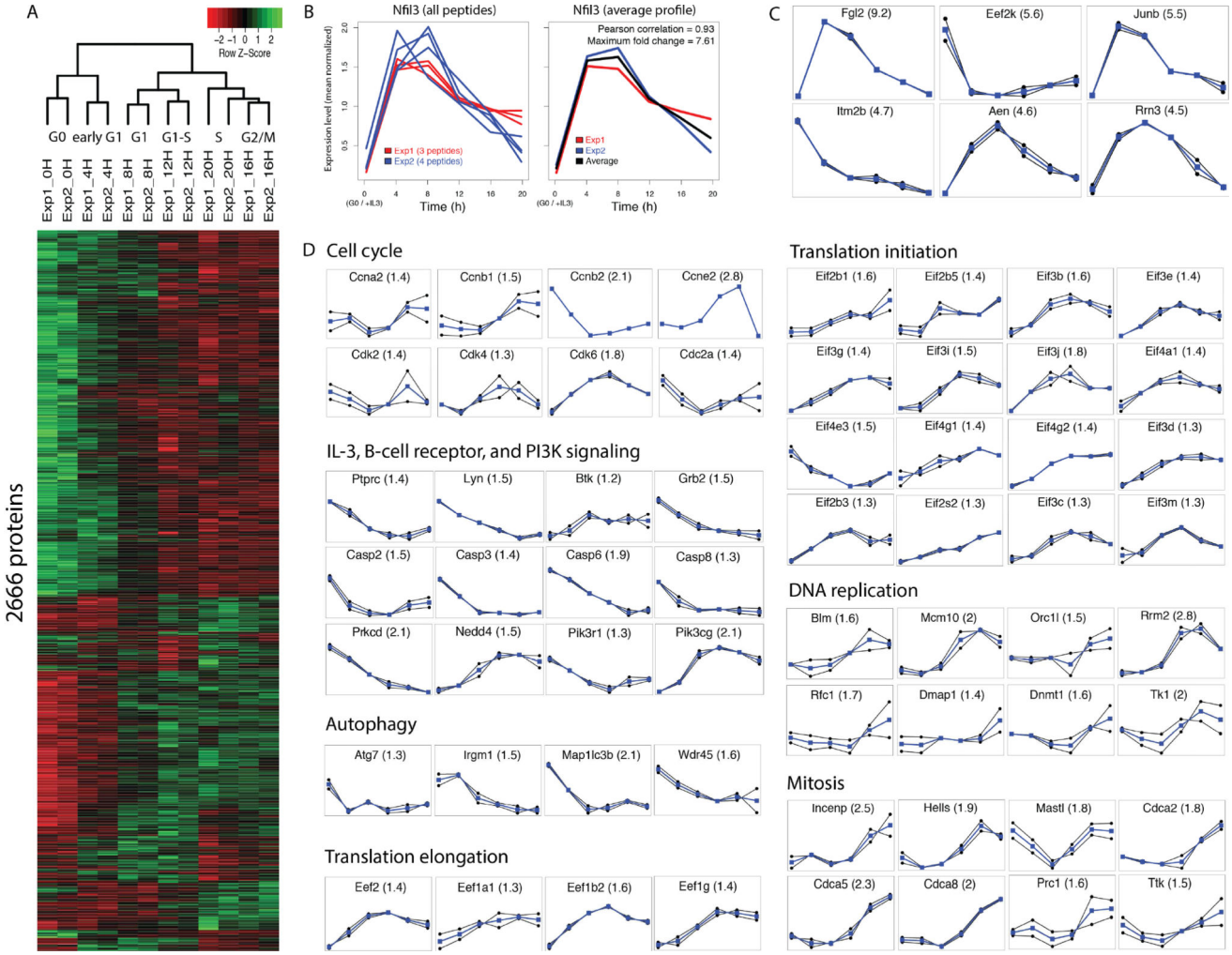

Figure 2. Proteomics data of temporal expression and highly confident individual proteins

The data are based on Pearson correlation coefficients (r) between all pairs of peptides from the duplicate experiments. (A) Unsupervised hierarchical clustering of 2,666 proteins whose expression profiles from duplicate experiments have r > 0.5. (B) A representative expression profile from our TMT data. The top second protein from A, Nfil3, is shown. It is a transcription factor which positively responds to IL-3. The left panel shows profiles of all peptides detected from our duplicate TMT experiments. The right panel shows their averaged profiles for the protein itself. Upon the IL-3 activation the expression level of Nfil3 was highly up-regulated as expected. We use averaged profiles for individual proteins in the subsequent main text. (C) Temporal expression profiles of the 6 highly confident proteins with MFC > 4. (D) Manually selected confident protein profiles for 7 cellular processes.

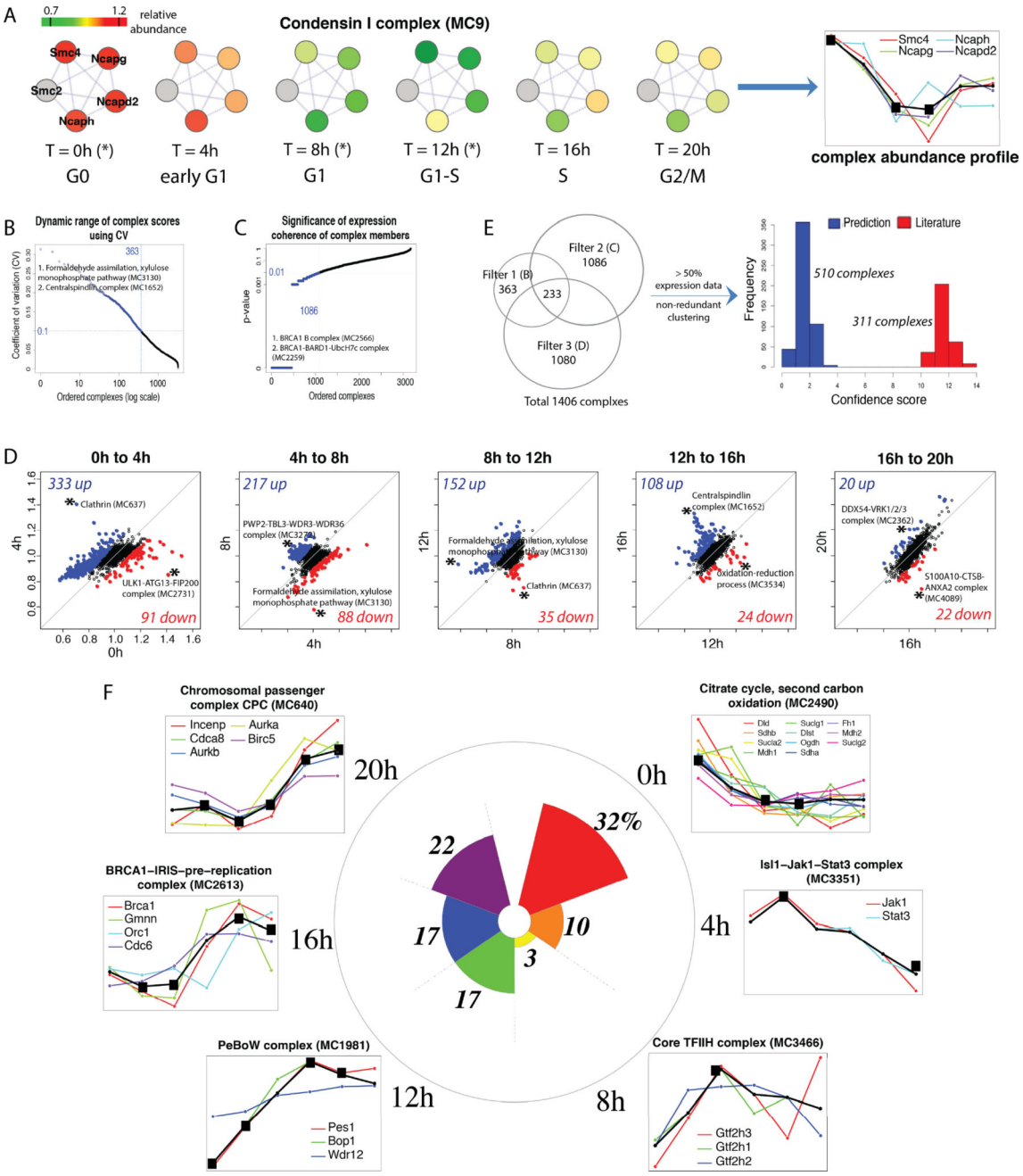

Figure 3. Analysis of multi-protein modules/complexes

(A) An example complex, condensin I complex (MC9), is shown to illustrate how the complex abundance profile is derived. Condesin I complex is composed of 5 proteins among which Smc2 (grey) was not detected in our TMT experiments. The relative abundance levels of the component proteins from the TMT data are color-coded at each time point. Then, the COMPLEAT tool generates the complex abundance profile (in black). The x-axis is for the 6 time points and the y-axis for mean-normalized abundance levels in an arbitrary unit. The black square means that a module score is enriched or statistically significant at a given time point with a p-value < 0.01. (B) A distribution of coefficient of variations (CV) of temporal

profiles of the 3177 significant modules. We chose a threshold of 0.1 to obtain 363 dynamic modules. The top 2 modules, formaldehyde assimilation, xylulose monophosphate pathway (MC3130) and centralspindlin complex (MC1652), are highlighted. (C) A distribution of p-values for expression coherence of component proteins in 3177 significant modules. We chose a threshold of 0.01 to obtain 1086 dynamic module. The top 2 modules, BRCA1 B complex (MC2566) and BRCA1-BARD1-UbcH7c complex (MC2259), are highlighted. (D) Scatter plots of fold changes of module scores at the adjacent time steps for 3177 significant modules. Based on the histogram of all fold changes, thresholds of 1.1 and 0.9 are chosen for up-regulation (in blue) and down-regulation (in red), respectively. The numbers of up-/down-regulated modules are shown along with the top up-/down-regulated modules (asterisked). (E) The final list of 821 dynamic modules is obtained from the union of the 3 sets of dynamic modules from B, C, and D. We retained only those modules more than 50% of whose component proteins have the TMT expression data, and then clustered to generate non-redundant modules. We focused on the 311 literature-supported modules (confidence score > 10) in this study. (F) The sector plot represents the fraction of modules whose scores become the maximum at each time point. Example module profiles are shown at all time points.

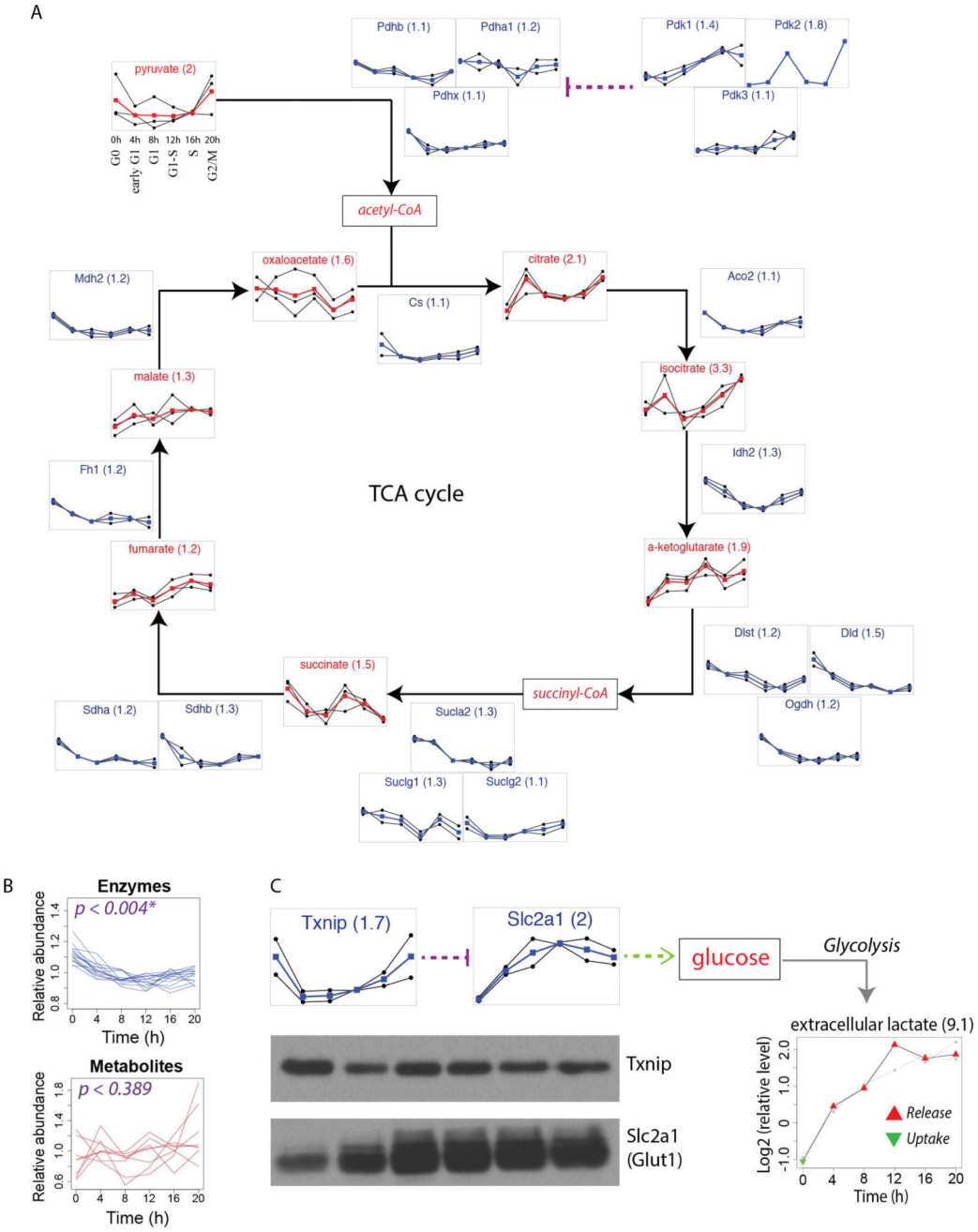

Figure 4. Down-regulation of the TCA cycle and up-regulation of glycolysis

(A) Schematic representation of the TCA cycle with temporal profiles of enzymes and metabolites detected. Enzymes are shown in blue (average) with duplicates in black and metabolites in red (average) with triplicates in black. The x-axis is the 6 time points and the y-axis mean-normalized abundance levels in an arbitrary unit. The number in the parentheses next to each molecule name shows the maximum fold change (MFC) over the 20 hours. (B) The average profiles of all 16 enzymes and metabolites in the TCA cycle. The enzyme profiles show a statistically significant coherent down-regulation ($p < 0.004$) unlike the metabolite profiles ($p < 0.389$). (C) Up-regulation of glycolysis was observed through

down-regulation of Txnip and up-regulation of Slc2a1 from the proteomics data and high release of lactate from the metabolomics data. Western blotting shows consistent expression patterns of Txnip and Slc2a1.

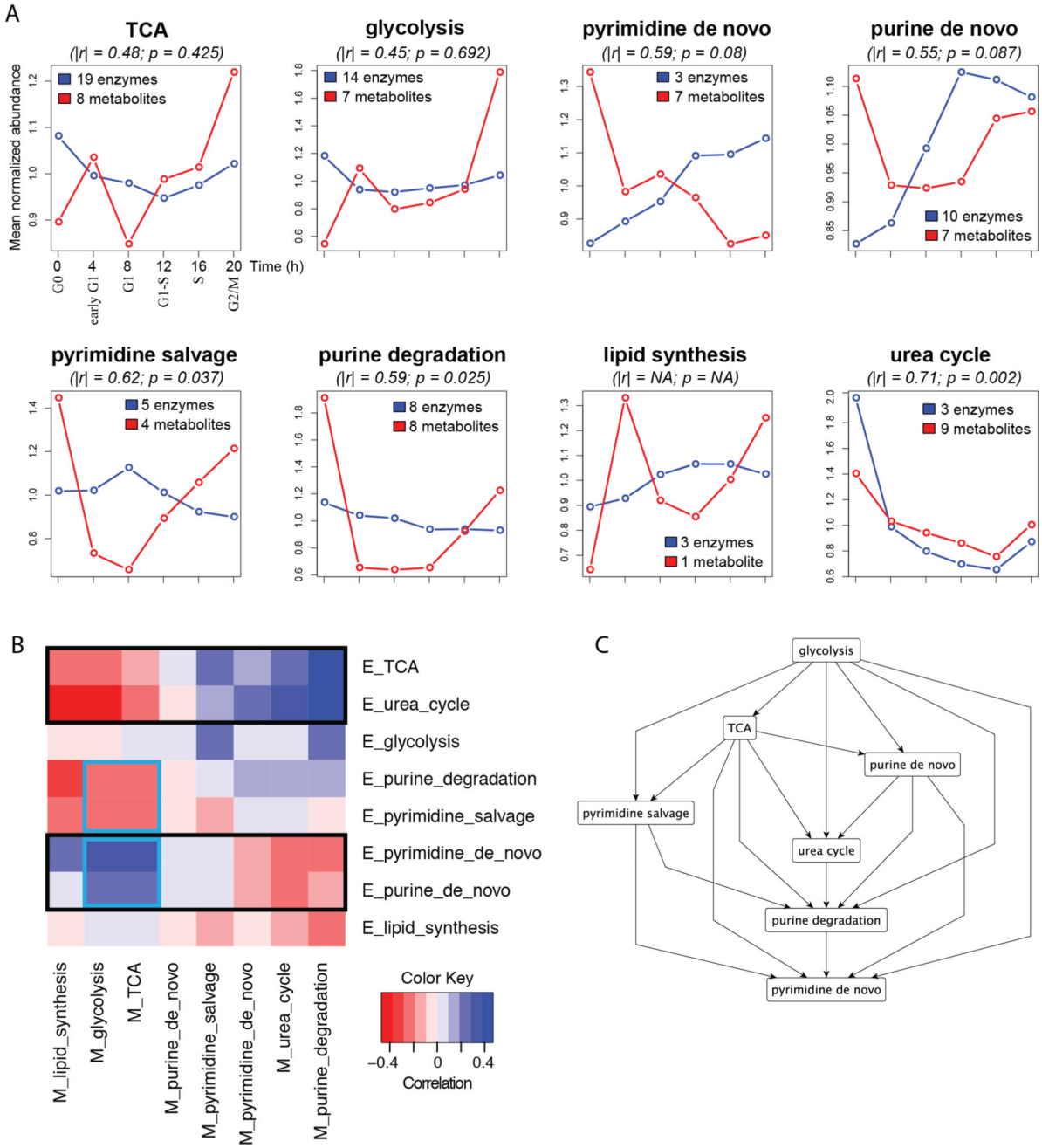

Figure 5. Correlation between enzymes and metabolites for each pathway and cross correlations among the pathways

(A) Average abundance profiles of all enzymes and metabolites for 8 pathways detected in our experiments. Enzyme profiles are in blue and metabolite profiles in red. All abundance levels are normalized to their mean values over the 20 hours. The average values of absolute Pearson correlation coefficients between enzymes and metabolites (|r|) and p-values (p) are also shown. Not available (NA) for lipid synthesis because it has only one metabolite measured (citrate). (B) A heatmap of enzyme-metabolite cross correlations. Notable correlation patterns are highlighted in the black and cyan boxes. “E_” for enzymes in rows and “M_” for metabolites in columns. (C) The network diagram shows cross-correlation

inter-relationships. The nodes represent pathways and a link from pathway 1 to pathway 2 is established if enzymes in pathway 1 have higher correlations with metabolites in pathway 2 than with metabolites in pathway 1 itself, on average. We take absolute Pearson correlations for this network for simplicity. Using this representation scheme, we built a hierarchical structure of pathway relationships. Note that glycolysis is located at the top of the structure connecting to all the other pathways. See Table S2 for all correlation values.

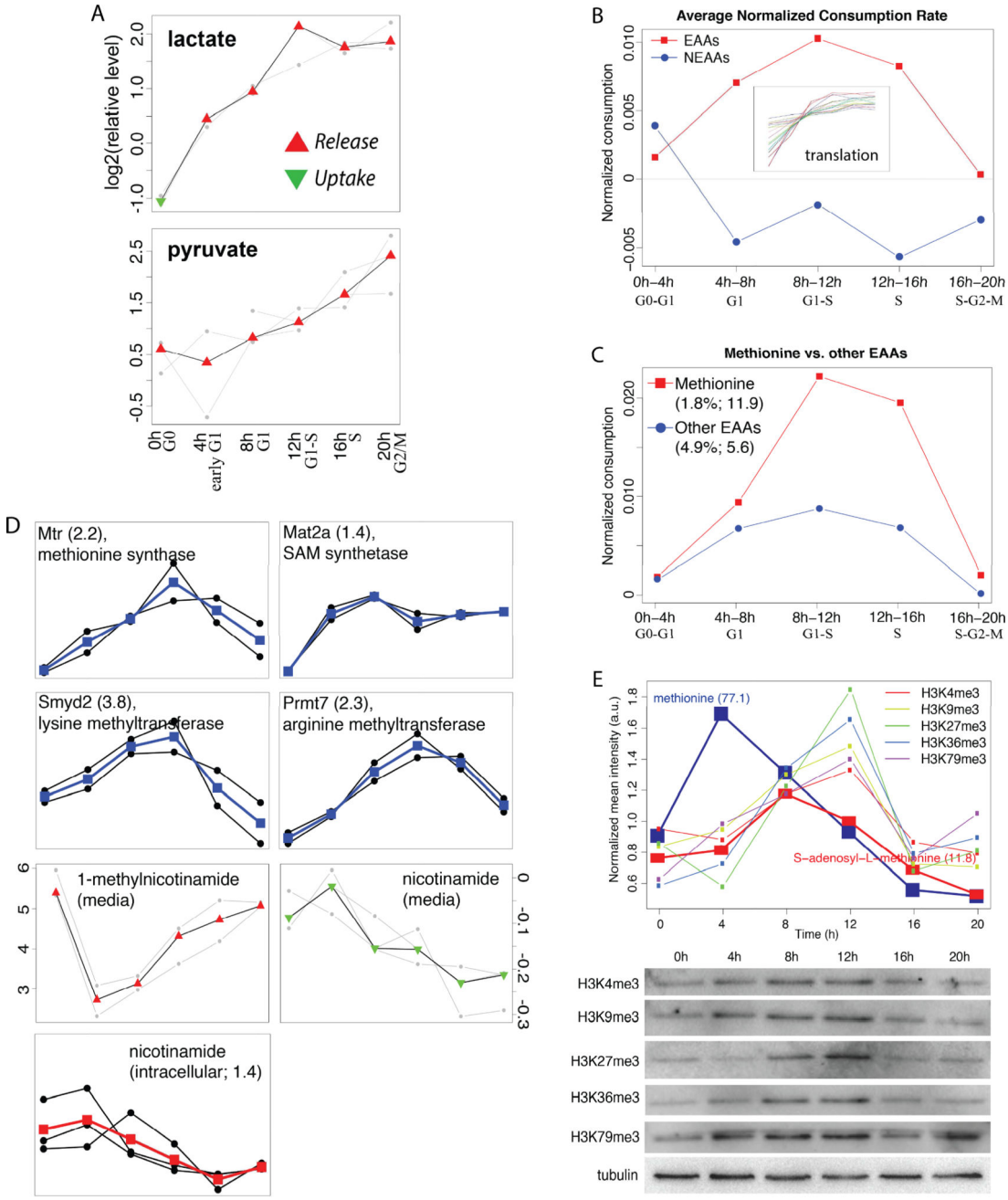

Figure 6. Media/extracellular metabolite profiling and methionine metabolism

(A) Temporal profiles of lactate and pyruvate. (B) Average normalized consumption rates of essential vs. non-essential amino acids (EAAs vs. NEAAs). The consumption of EAAs is correlated with up-regulated protein profiles involved in translation. (C) Normalized consumption rates of Met and the other 8 essential amino acids. The numbers in the legend represents the relative frequency and the fold change of the consumption rates at 8h–12h and 0h–4h. (D) Protein and metabolite profiles involved in Met metabolism. (E) Intracellular levels of 5 histone tri-methylation marks were measured using Western blot and quantified by normalizing to tubulin levels. The normalized levels were compared with intracellular

abundance patterns of Met and SAM in an arbitrary scale for simplicity with MFC values in parentheses.

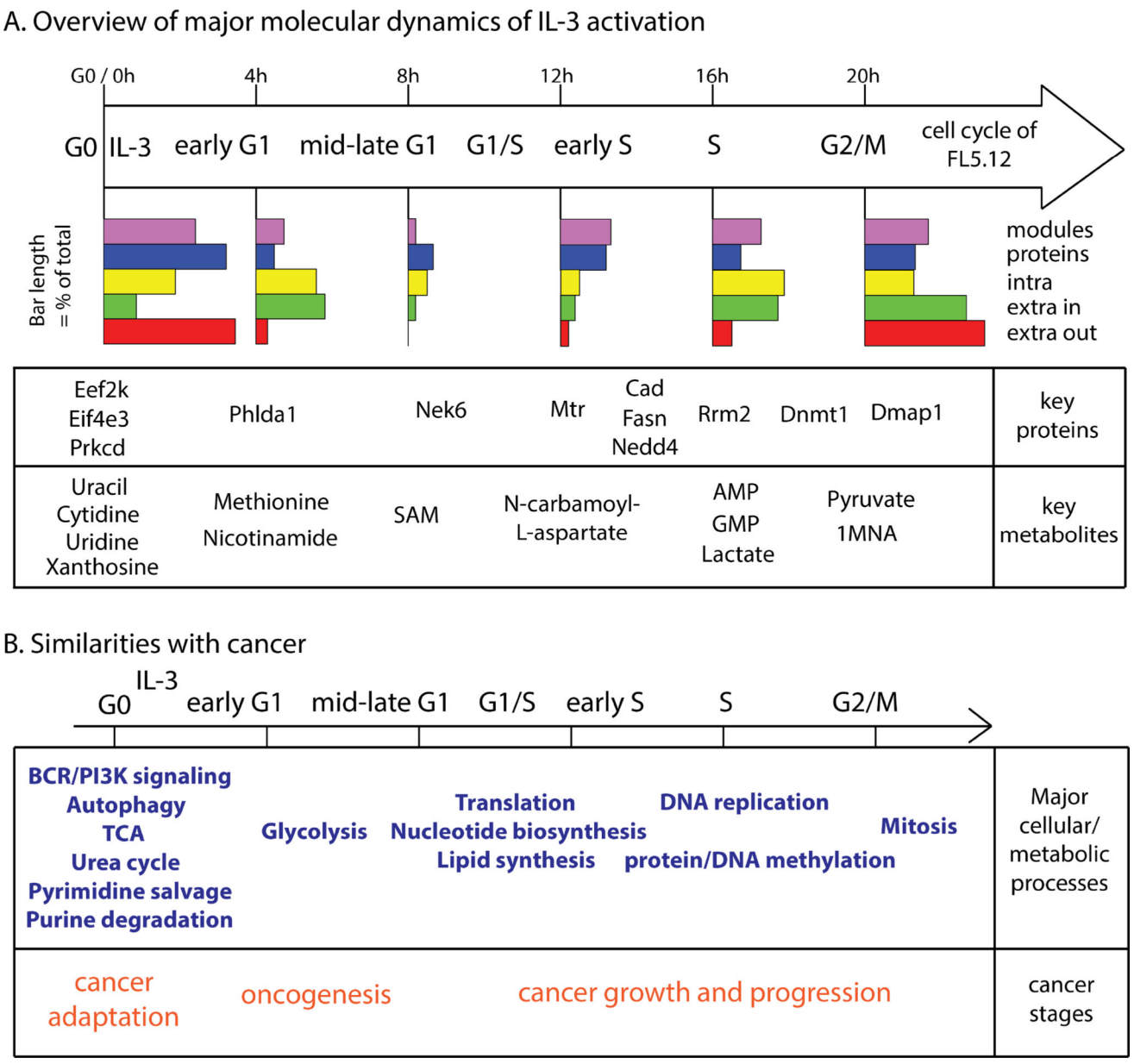

Figure 7. A model of IL-3 activation of FL5.12 cells and a relationship to cancer studies

(A) An overview of molecular dynamics from our proteomics and metabolomics data of IL-3 activation in terms of 5 classes of most abundant molecules across the cell cycle phases. Each color bar at each time point represents a relative fraction (or percentage) of molecules in each class of the same color (100%) that have the maximal abundance at that time point, showing temporal distributions of most abundant molecular fractions in each class. We only selected those molecules in each class whose MFCs are greater than their median values, i.e., the top 50%. The 5 classes are: protein complexes/modules in purple (“modules”), individual proteins in blue (“proteins”), intracellular metabolites in yellow (“intra”), uptaken extracellular metabolites in green (“extra in”), and released extracellular metabolites in red (“extra out”). The median MFCs of the 5 classes are 1.24, 1.37, 2.49, 1.3, and 1.66, respectively. Several key proteins and metabolites with maximal abundance at each time

point are shown in the table. (B) Our model with major cellular and metabolic processes most affected or active across the cell cycle phases showing similarities with the typical cancer stages.